Hadamard acquisition of 13C-13C 2D correlation NMR spectra

Piotr Paluch, Eriks Kupce, Julien Trebosc, Olivier Lafon, Jean-Paul Amoureux

Hadamard acquisition of ^{13}C-^{13}C 2D correlation NMR spectra

Piotr Paluch,[1,3] Ēriks Kupče,[2] Julien Trébosc,[3,4] Olivier Lafon,[3,5] Jean-Paul Amoureux[3,6,7,*]

[1] Centre of Molecular and Macromolecular Studies, Polish Academy of Sciences, 112 Sienkiewicza, PL-90363 Lodz, Poland.
[2] Bruker UK Ltd., Banner Lane, CV4 9GH Coventry, UK.
[3] Univ. Lille, CNRS-8181, Unit of Catalysis and Chemistry of Solids, F-59000 Lille, France.
[4] Univ. Lille, CNRS-2638, Fédération Chevreul, F-59000 Lille, France.
[5] Institut Universitaire de France, 1 rue Descartes, F-75231 Paris, France.
[6] Bruker Biospin, 34 rue de l'Industrie, F-67166 Wissembourg, France.
[7] Riken NMR Science and Development Division, Yokohama, 230-0045 Kanagawa, Japan.

* Corresponding author: jean-paul.amoureux@univ-lille.fr

Keywords: solid-state NMR, selective excitation, Hadamard encoding, 2D spectra, ^{13}C-^{13}C HOMCOR.

Abstract. We show that a multi-selective excitation with Hadamard encoding is a powerful tool for 2D acquisition of ^{13}C-^{13}C homo-nuclear correlations. This method is not designed to improve the sensitivity, but rather to reduce the experiment time, provided there is ***sufficient sensitivity***. Therefore, it allows fast acquisition of such 2D spectra in labeled molecules. The technique has been demonstrated using a U-^{13}C-^{15}N histidine hydrochloride monohydrate sample allowing each point of the build-up curves of the ^{13}C-^{13}C cross-peaks to be recorded within 4 min 35 s, which is very difficult with conventional methods. Using the U-^{13}C-^{15}N f-MLF sample we have demonstrated that the method can be applied to molecules with fourteen ^{13}C resonances with a minimum frequency separation of 240 Hz.

I. Introduction

Most modern NMR (Nuclear Magnetic Resonance) multi-dimensional experiments are based on the recording of an ensemble of free induction decay (FID) signals that are excited by a sequence of hard non-selective radio-frequency (rf) pulses. The frequency spectra are then obtained by applying a Fourier Transform (FT) along all dimensions. However, this type of signal acquisition requires accumulating numerous FIDs, especially in the case of well crystallized solid compounds producing narrow resonances that are spread over large frequency ranges. For example, this is the case when one of the indirect dimensions encodes the ^{13}C isotope. Indeed, on one hand the step in this indirect dimension, Δt_1, which is usually constant, must be small enough to observe the large frequency range, $\Delta\nu_{0,max}$ ($\Delta t_1 < 1/\Delta\nu_{0,max}$), and on the other hand the maximum evolution time along the indirect dimension must be long enough to achieve a sufficient resolution to distinguish between close resonances separated by $\Delta\nu_{0,min}$ ($t_{1,max} \geq 1/\Delta\nu_{0,min}$). Globally, this type of acquisition requires numerous steps in the indirect dimensions, and hence very long accumulation times. In the case of big molecules, such as proteins, the main way to decrease the acquisition time is to use non-linear sampling of the indirect dimensions, which allows gaining approximately a factor of two in time for each indirect dimension.[1–3]

However, for small molecules with a limited number of resonances (i.e. sparse spectra), another type of multi-dimensional acquisition can be used. In this case, the broadband excitation of all species in the indirect dimensions is replaced with multiple-selective excitations combined with some sort of frequency encoding, e.g. Hadamard or phase encoding

[4,5]. Obviously, this approach requires prior knowledge of the resonance frequencies along the indirect dimensions After this selective frequency excitation and acquisition of the individual spectra, the full multi-dimensional spectrum may then be re-constructed by using this ensemble of spectra and the prior knowledge of the resonance frequencies and line-shapes along the indirect dimensions.[6].

Up to now this selective methodology has been mainly applied to 2D experiments in liquids.[4–7]. It has been demonstrated that in the case of sensitive experiments performed on small molecules presenting a limited number of resonances, *m*, this selective excitation technique allows recording fast 2D spectra because of the much smaller number of 1D FIDs to be acquired: *m* instead of $2t_{1,max}/\Delta t_1 = 2\Delta\nu_{0,max}/\Delta\nu_{0,min}$ with conventional 2D methods. The factor of 2 comes from the sign-discrimination required with the FT methods. This problem does not occur with selective excitation experiments because of the prior knowledge of the resonance frequencies. An additional gain in S/N ratio of up to $\sqrt{m}$ is obtained by replacing the *m* sequential individual single-selective pulses (SSP) with *n* multi-selective pulses (MSP, $n \geq m$). Most of the time, the two types of selective pulse sequences (SSP and MSP) are related through an encoding Hadamard square matrix of size n (called H_n hereafter), consisting of 0 and 1 (or ±1) coefficients. The FIDs corresponding to all SSP can afterwards be retrieved from those recorded with MSP with the same H_n matrix. The optimum size *n* of the H_n matrix is the multiple of 4 which is just larger than the number *m* of resonances.

It must be noted that with respect to the conventional broad-band excitation, the gain in S/N per unit of time afforded by the use of SSP is limited to $\sqrt{2}$, due to sign-discrimination. Therefore, the gain in time provided by the use of much less t_1 steps is mainly useful in the case of sensitive experiments. In this 'sampling limited' case, it allows obtaining new information with an acceptable S/N that is hardly accessible with the conventional methods due to too long acquisition times, e.g. those related to build-up curves. In the case of 'sensitivity limited' experiments, numerous accumulations are always required, independently of the number of t_1 steps used, and this type of information is hardly accessible anyway.

The 2D acquisition with Hadamard encoding has been previously used to record at moderate magic-angle spinning (MAS) speeds (ν_R = 15-19 kHz) either single-quantum to single-quantum (SQ-SQ) DARR ^{13}C HOMCOR (Homo-nuclear Correlation) or ^{1}H→^{13}C CPMAS HETCOR (Hetero-nuclear Correlation) spectra of U-^{13}C amino-acids.[8] It has also been used more recently to record ^{13}C-^{15}N HETCOR spectra of U-^{13}C-^{15}N f-MLF at ν_R = 13 kHz [9] or to measure ^{13}C-^{13}C scalar couplings.[10] In this communication, we show how this Hadamard encoded acquisition can also be used to record ^{13}C-^{13}C 2D HOMCOR spectra at the much higher spinning speed of ν_R = 62.5 kHz.

II. ^{13}C-^{13}C HOMCOR sequences

We have chosen implementing the Hadamard encoding/decoding with multi-selective pulses (MSP) and three different ^{13}C HOMCOR sequences with SQ-SQ observation, usable at ultra-fast MAS: RFDR,[11–13] CP^3,[14–19] and DQF-BR2$^1_2$ (double-quantum-filtered BR2$^1_2$).[20–22] The sequences are shown in Fig.**1** and for each of them the part corresponding to the ^{1}H channel is only shown once at the top as it is the same for the conventional and the Hadamard versions. It must be noted that the CP^3 sequence (Figs.**1e**,**f**) can only be used with protonated samples, whereas the two other schemes can always be used, with or without the initial CPMAS signal enhancement and the ^{1}H decoupling.

In theory, for each ^{13}C resonance one may optimize the pulse selectivity according to its closest ^{13}C resonance. However, this would lead to different selective pulse lengths, and hence to different signal attenuations during the selective pulses for the various resonances.

Moreover, even in this setup, the total duration of the encoding waveform would still be defined by the longest encoding element. Therefore, we see such an approach as hardly practical and we have used a common selective pulse length, τ_{sp}, corresponding to the most selective component. For each single-selective pulse (SSP), we have used a Gaussian line-shape, truncated at 10 % to limit the losses occurring during these long excitations. The multi-selective pulses (MSP) have been generated by the Bruker WaveMaker software, which also allows calculating the multi-excitation profiles of the rf-pulse-shapes.

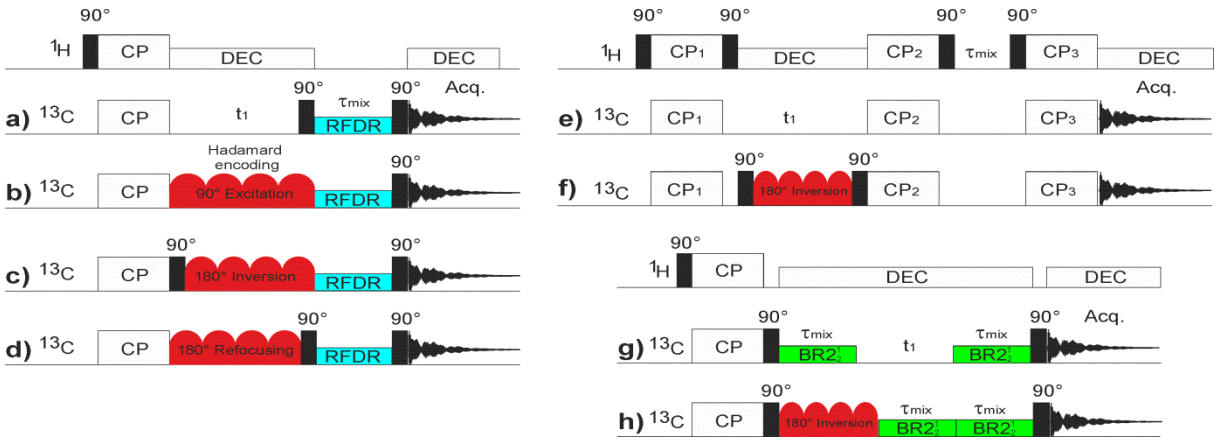

Fig.1. ^{13}C-^{13}C HOMCOR sequences. (a-d) SQ-SQ RFDR with: (a) only HPs (conventional), (b) π/2-MSP, (c) inverting and (d) refocusing π-MSP. SQ-SQ CP^3 with: (e) only HPs (conventional), (f) inversion π-MSP. (g) DQ-SQ conventional $BR2^1_2$ with only HPs. (h) SQ-SQ DQF-$BR2^1_2$ with inversion π-MSP. Black boxes are π/2 HP.

II.1. RFDR

In Fig.**1a-d**, we show the RFDR (Radio-Frequency-Driven Recoupling)[11–13] pulse sequences used in this article; either with conventional acquisition (Fig.**1a**) or with Hadamard encoding (Fig.**1b-d**). In Fig.**1a**, after the $^1H \rightarrow ^{13}C$ CPMAS initial transfer, the ^{13}C magnetization is transverse and can evolve during t_1. Then, this magnetization must be stored along z because RFDR is a zero-quantum recoupling. This scheme consists of rotor-synchronized π-pulses, and at ultra-fast MAS the $(XY8)4^1$ super-cycling has been shown to be optimized for ^{13}C-^{13}C interactions.[11] There are several ways of introducing a selective excitation with RFDR, which implies replacing the t_1 delay and the following π/2 storing hard-pulse (HP) on the ^{13}C channel. The simplest one employs a π/2-MSP (Fig.**1b**), and the second involves a π/2-HP positioned either before (Fig.**1c**) or after (Fig.**1d**) the π-MSP. In Fig.**2** we show the six rows of histidine hydrochloride monohydrate, recorded with the three versions of 2D H_8-RFDR sequences. One observes that the two most efficient methods use a π-MSP for either inversion or refocusing purposes (Fig.**1c** and **d**), respectively. Sequences using a π/2-MSP are less efficient than those using a π-MSP because their selective pulse length is twice longer for the same selectivity, here τ_{sp} = 3.6 and 1.8 ms respectively for 500 Hz bandwidth, which leads to larger losses. By comparing in detail the spectra shown in Fig.**2**, one notices that the selective inversion is on average slightly more efficient than the refocusing. Therefore, in the following we have chosen to use only selective inversion π-MSP, as shown in Fig.**1c**,**f**,**h**.

II.2. CP^3

This HOMCOR sequence uses three CPMAS ^1H-^{13}C transfers (Fig.**1e**), and hence is called CP^3 or CHHC when describing the transfer of magnetization.[14–19] After the initial CP_1

transfer, the total ^{13}C magnetization evolves in the *xy* plane during t_1. A second CP_2 step transfers the t_1 modulated magnetization back to the protons. The ^{1}H magnetization is then stored along the $\boldsymbol{B}_0$ magnetic field by a $\pi/2$-pulse. The distribution of ^{1}H longitudinal magnetization is then allowed to equilibrate during a spin diffusion mixing period, τ_{mix}. With another $\pi/2$-pulse, the ^{1}H polarization is restored in the *xy* plane and a final CP_3 step is applied for high-resolution ^{13}C detection. It is important to note that the ^{1}H transverse magnetization that is not transferred through the ^{13}C channel during t_1 must be perfectly purged before the CP_2 step. Therefore, just after CP_1 the residual transverse spin-lock ^{1}H magnetization is sent back to the *z*-axis with the 2nd ^{1}H $\pi/2$-HP. However, due to rf-inhomogeneity this pulse is not perfect, and the transverse ^{1}H magnetization remaining after the 2nd $\pi/2$-HP must be cancelled by cycling the phase of the initial ^{1}H $\pi/2$-HP, relative to the phase of the ^{1}H spin-lock pulse of CP_2. So, generally the efficient polarization transfers between ^{1}H nuclei can be combined with the superior spectral resolution of ^{13}C nuclei in a 2D HOMCOR correlation spectroscopy experiment. The conventional CP^3 sequence is shown in Fig.**1e**, and the selective version in Fig.**1f**.

II.3. DQF-BR2$_2^1$

The main disadvantage of the two previous SQ-SQ experiments is the fact that the signal contributions on the diagonal have no physical meaning, because they are the sum of the auto-correlation signals and of those arising from spins which do not take part in transfer processes. The second contributions are usually much larger than the first ones, especially for short mixing times. Practically, this means that spatial proximities are impossible to analyze between carbons that are of the same species but in different molecules and difficult with species with close resonance frequencies. These limitations can be overcome by using DQ-SQ experiments, in which the DQ-correlated states are detected along the indirect dimension (e.g. Fig.**1g**).[20–22] Unfortunately, it is difficult to perform a selective excitation in such DQ-SQ experiments. Indeed, each excitation should be double-selective to only excite one pair of spins, not a single spin as with previous SQ-SQ experiments. Moreover, the number of such double-selective excitations should be (*n*-1)/2 higher than with SQ-SQ experiments: *n*(*n*-1)/2 instead of *n*. Therefore, we have chosen using a compromise between pure SQ-SQ and DQ-SQ experiments, and used a SQ-SQ one with DQ-filtering. The filter ensures that all signals observed in the 2D spectrum arise from spins that have passed through a DQ coherence in the course of the recoupling procedure. In this way, signal contributions from spins which have not at all been involved in transfer processes are removed from the diagonal of the spectrum. However, the auto-correlation signal located on the diagonal is superimposed with signal contributions from other correlations. We have used the BR2$_2^1$ recoupling (Fig.**1h**), but it must be mentioned that other such sequences have been proposed, such as the Sp ones (p = 2-4).[23,24] It should be noted that the BR2$_2^1$ recoupling scheme can also be applied to half-integer spin quadrupolar nuclei.[25,26]

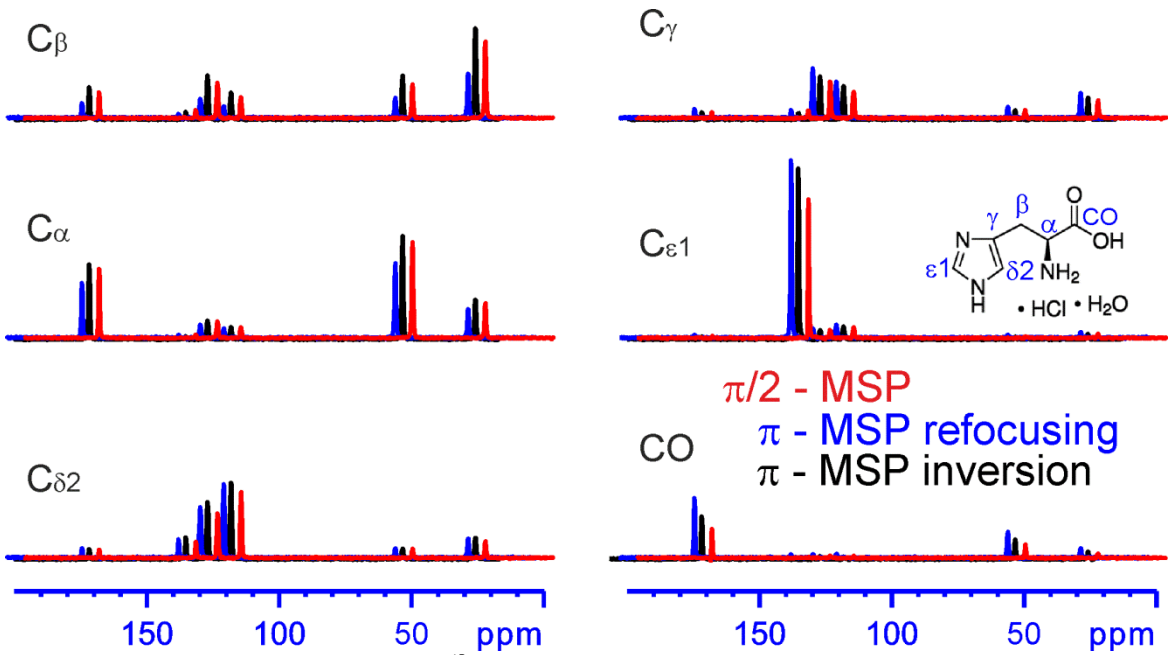

Fig.2. Rows from the 2D RFDR spectra of U-^{13}C labeled histidine hydrochloride monohydrate recorded with the 3 different MSP used with H_8-RFDR and a selective excitation bandwidth of BW_{FWHM} = 500 Hz, which corresponds to a pulse length of τ_{sp} = 1.8, 1.8 and 3.6 ms for: 180° inversion (Fig.**1c**), 180° refocusing (Fig.**1d**) and 90° excitation (Fig.**1b**), respectively. B_0 = 18.8 T, ν_R = 62.5 kHz, τ_{mix} = 8 ms, NS = 64, RD = 2 s, and T_{exp} = 18 min 25 s for each 2D.

III. Tests on U-^{13}C histidine hydrochloride monohydrate.

The experiments have been recorded at 18.8 T with a spinning speed of ν_R = 62.5 kHz (∅ = 1.3 mm). Full details of experiments setup have been provided in ESI. The ^{13}C shifts are referenced with respect to TMS. The main use of Hadamard ^{13}C-^{13}C HOMCOR 2D spectra is to record fast the build-up curves of labeled samples. To test this possibility, we have first recorded a large series of 2D spectra on U-^{13}C histidine hydrochloride monohydrate. This compound contains 6 different carbon species, and hence we have used an H_8 Hadamard encoding matrix. In the following, the peak intensities are normalized with respect to the highest signal in the series of spectra.

III.1. Optimization of the selective pulse-length

The first parameter to optimize is the length, τ_{sp}, of the selective pulses. Indeed, this pulse must be long enough to selectively excite only one resonance at a time, but not too long because of the relaxation losses occurring during this pulse. It must be reminded that the excitation bandwidth is inverse proportional to the pulse-length, $BW_{FWHM} = A/\tau_{sp}$, with A = 0.9 or 1.8 in the case of 10% truncated Gaussian line-shapes for π or π/2 pulses, respectively. An easy such optimization of the pulse-length is obtained by (i) fixing the mixing time to a very small value to theoretically only observe SQ-SQ diagonal peaks, and (ii) recording a 1D spectrum with selective excitation of one of the two carbons that are with the minimum frequency separation. In Fig.**3**, we show six such 1D H_8-RFDR spectra for the C_γ of histidine hydrochloride. Due to the decrease of the pulse-length and the associated losses, the auto-correlation peak amplitude increases with the bandwidth up to BW_{FWHM} = 500 Hz. One or two negative cross-peak are observed with BW_{FWHM} = 750, 1000 or 1500 Hz, respectively, which means that one or two very close resonances are also partially excited. In the following, we have chosen BW_{FWHM} = 500 Hz. It must be noted that when they are excited, the closest resonances always appear with negative sign because of the off-resonance irradiation.

Therefore, in the case of very large losses, which may occur with slow spinning speeds, for which using the shortest as possible selective pulse length is recommended, one way to gain in S/N ratio is to use a BW_{FWHM} value slightly larger that optimum, and to only take into account the cross-peaks with positive amplitudes. For example, at slow spinning speed using BW_{FWHM} = 1500 Hz should allow to decrease the pulse length to τ_p = 600 µs.

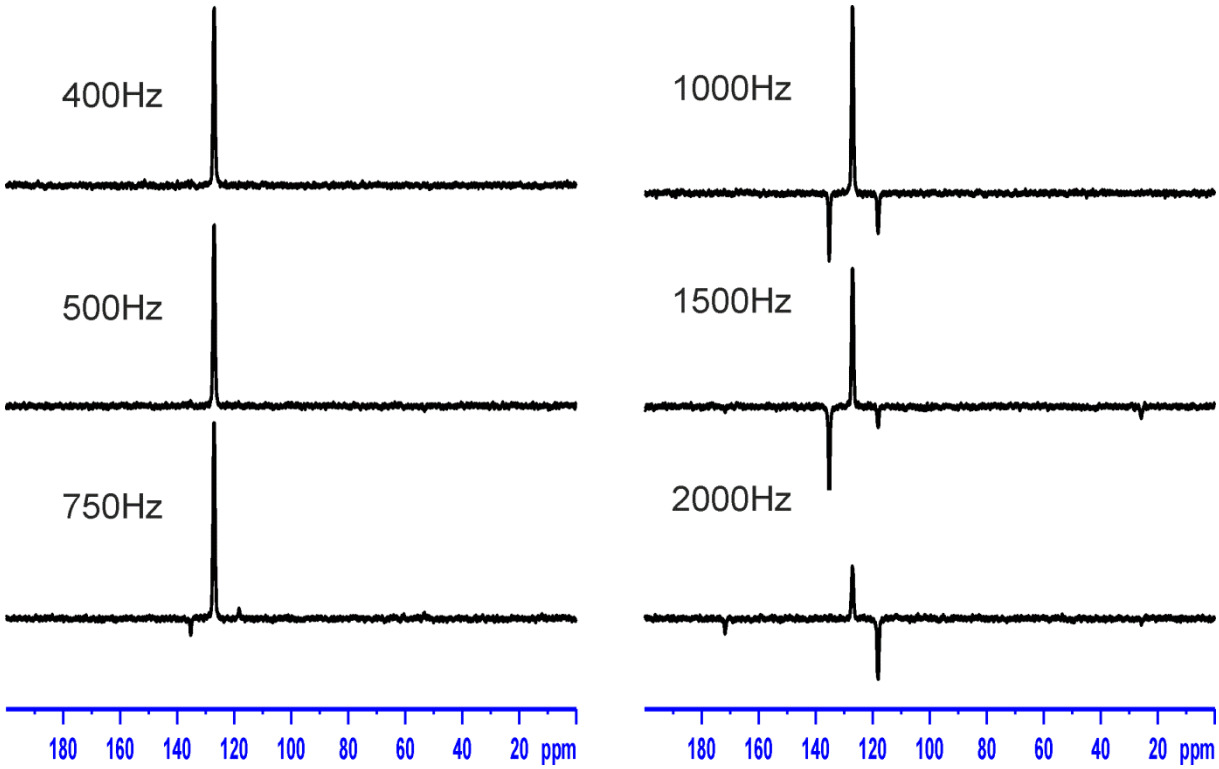

Fig.3. U-^{13}C histidine hydrochloride monohydrate. 1D H_8-RFDR spectra recorded with τ_{mix} = 16 µs (negligible ^{13}C-^{13}C transfer), for C_γ with bandwidth indicated on the spectra. NS = 16, RD = 2s, T_{exp} = 4min 35s for each 2D.

III.2. Build-up curves

We have then recorded a series of 2D SQ-SQ spectra, as the three ones shown in Fig.**S1**, for the three different HOMCOR schemes, versus the mixing time up to τ_{mix} = 13 ms. For such a labeled compound, each Hadamard 2D spectrum was acquired in only 4 min 35 sec. In Fig.**4** we show the build-up curves corresponding to C_α (Fig.**4a**-**c**) or $C_{\delta 2}$ (Fig.**4d**-**f**) carbon atoms. These build-up curves present different evolutions, which specify their use.

* For RFDR and CP[3] experiments (Figs.**4a**,**b**,**d**,**e**), the amplitudes of the diagonal peaks are largely predominant for small mixing times. However, the analysis of these diagonal peaks is useless because a large part of their intensities has no physical meaning and is not related to inter-nuclear distances. Only the cross-peak build-up curves can thus be used for structural analyzes. This limitation impedes the use of SQ-SQ experiments for species with close or equal resonance frequencies. This constraint is emphasized by the use of selective excitations which can hardly select very close resonances.

* For DQF-BR2$_2^1$ experiments, all build-up curves start from zero, because they all are related to dipolar transfers. However, only those of the cross-peaks are directly related to inter-nuclear distances. Indeed, the build-up curves of diagonal peaks (e.g. C_α) are related to auto (C_α-C_α) and hetero (C_α-C_β and C_α-C_O) correlations. Nevertheless, the auto-correlation build-

up curves can be retrieved qualitatively by subtracting the hetero-correlation signals to the diagonal one. Moreover, it must be noted that the cross-peaks of nearby resonances, which are close to the diagonal, are easier to detect than with the two other methods because the diagonal peaks are much smaller, especially for small mixing times. However, the limitation related to the selective excitation of species with close resonance frequencies remains.

* For RFDR and CP^3 experiments, the contact between the various carbons can be obtained through the ^{13}C-^{13}C (RFDR) or ^{1}H-^{1}H (CP^3) spin-diffusion process. Because the homo-nuclear dipolar interactions are ca. 16 times smaller with ^{13}C than with ^{1}H, the build-up curve variations are faster with CP^3 than with RFDR (compare Fig.**4a** and **b**). For example, in Fig.**4b**,**e** they mainly occur up to $\tau_{mix} \approx 500$ µs for CP^3, and afterwards only plateaus are observed for the cross-peaks so that a slow decrease is observed for the diagonal peaks.

* One observes that the amplitudes of some CP^3 cross-peaks are not zero with $\tau_{mix} = 0$ (e.g. C_α-C_β in Fig.**4b**). This signal is related to the ^{1}H-^{1}H spin-diffusion occurring during the three CPMAS transfers.

* The DQF-$BR2_2^1$ evolution is faster than that with RFDR.

* As a result, the analysis of the build-up curves of these three ^{13}C-^{13}C sequences can be limited to e.g. $\tau_{mix} \leq$ 3-4 ms.

We have tried to verify the build-up curves observed with Hadamard MSP excitation with those obtained in a conventional way. We have used the DQF-$BR2_2^1$ recoupling and tried to record the 2D spectra corresponding to the 24 mixing times used in Figs.**4c** and **f** in the limited total time of 24 hrs. However, to respect this time limitation we had to largely limit the indirect evolution time, hence leading to a large broadening of the resonances, which limited the number of cross-peaks that could be resolved. We show in Fig.**4c** the results that could be exploited for C_α. The other mixing times lead to too small and too broad resonances to be used. It was not possible to obtain any build-up curve for $C_{\delta 2}$ due to limited resolution. Actually, a roughly 10 times longer evolution time would have been required to obtain a usable resolution, thus leading to ca. 10 hours for each mixing time (Fig.**S2**). Nevertheless, these conventional results shown in Fig.**4c** demonstrate the correctness of the build-up curves obtained with Hadamard MSP excitation in a much smaller experiment time: 4 min 35 s instead of several hours.

As a conclusion, the CP^3 scheme should be used to analyze mostly the proximities of CH, CH_2 or CH_3 moieties, with the high-resolution of carbons, which is advantageous at moderate MAS speeds. The two other methods, RFDR and DQF-$BR2_2^1$, directly analyze the ^{13}C-^{13}C proximities. RFDR is approximately twice more efficient than $BR2_2^1$, but it does not allow analyzing auto-correlations and distances between nuclei with very close resonance frequencies; especially with selective excitation.

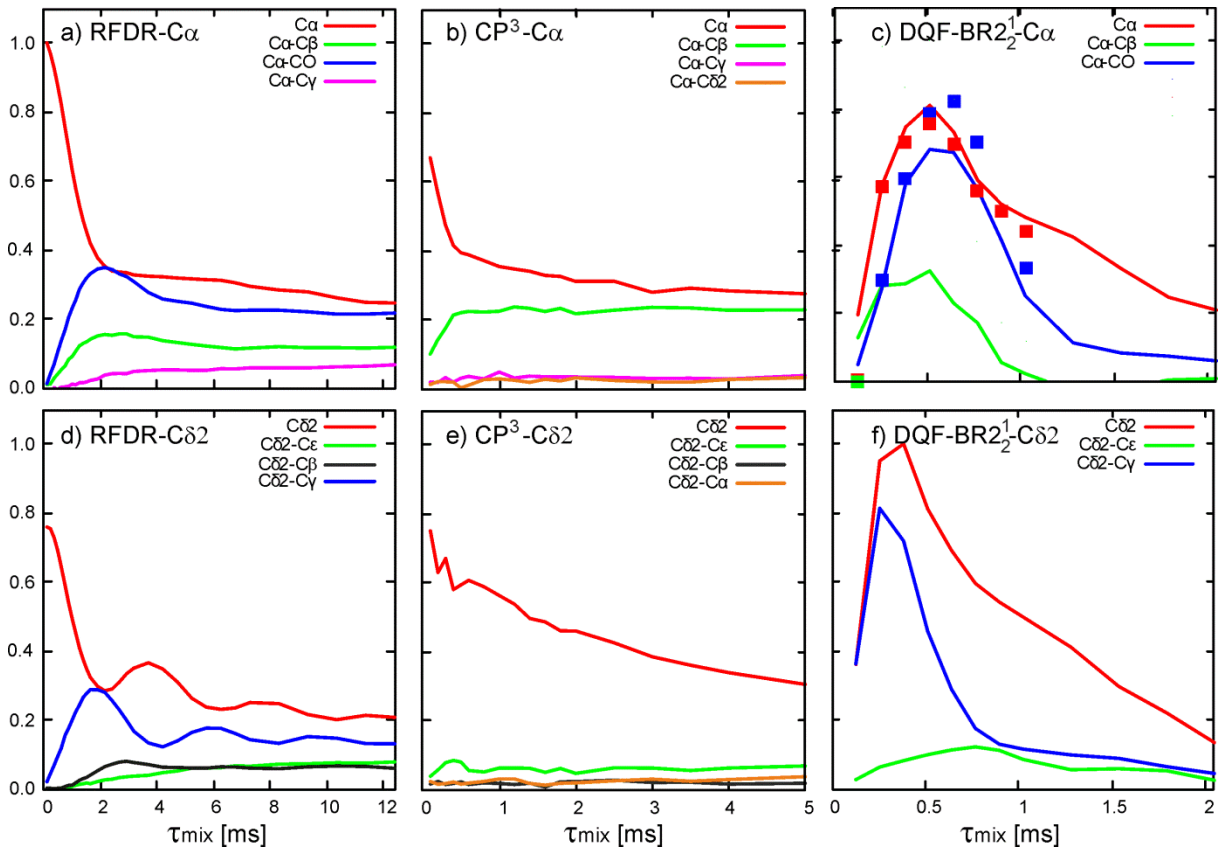

Fig.4. U-^{13}C histidine hydrochloride monohydrate. Build-up curves of C_α (a-c) or $C_{\delta 2}$ (d-f) versus τ_{mix}, for H_8-RFDR (a,d), H_8-CP^3 (b,e) and H_8-DQF-BR2$^1_2$ (c,f). BW_{FWHM} = 500 Hz, NS = 16, RD = 2s, T_{exp} = 4 min 35s for each 2D. In (c) we present as squares the intensity of C_α-C_α and C_α-C_O cross-peaks recorded in 1hr for each point with the conventional experiment.

IV. Tests on U-^{13}C/^{15}N f-MLF

As a second test sample, we have chosen a bigger molecule, the labelled f-MLF tri-peptide, N-formyl-Met-Leu-Phe (U-^{13}C-^{15}N f-MLF). The molecule and the 1D CPMAS ^{13}C spectrum are shown in Fig.**5**. The sample contains 19 different ^{13}C species and their isotropic chemical shifts, measured with an unlabeled sample, are given in Table.**S1**.[27,28] It must be noted that in Fig.**5b**, most of the ^{13}C resonances are broadened by the $^1J_{13C\text{-}13C}$ couplings in this quasi-fully labeled sample, and e.g. $L^{\delta 1}$ and L^{γ} resonances overlap, whereas they are discernible with unlabeled samples. Moreover, the F^{myl} formyl carbon is not observed because it is not labelled in our sample. Finally, aromatic carbons (F^{ε} and F^{δ}) are broadened by 180° flips of the phenyl ring and hence they cannot be cleanly separated at room temperature, and furthermore, they overlap with the F^{ζ} resonance. As a result, only 14 resonances are well resolved in Fig.**5b**, and hence we have used an H_{16} Hadamard encoding matrix for the multi-selective excitation.

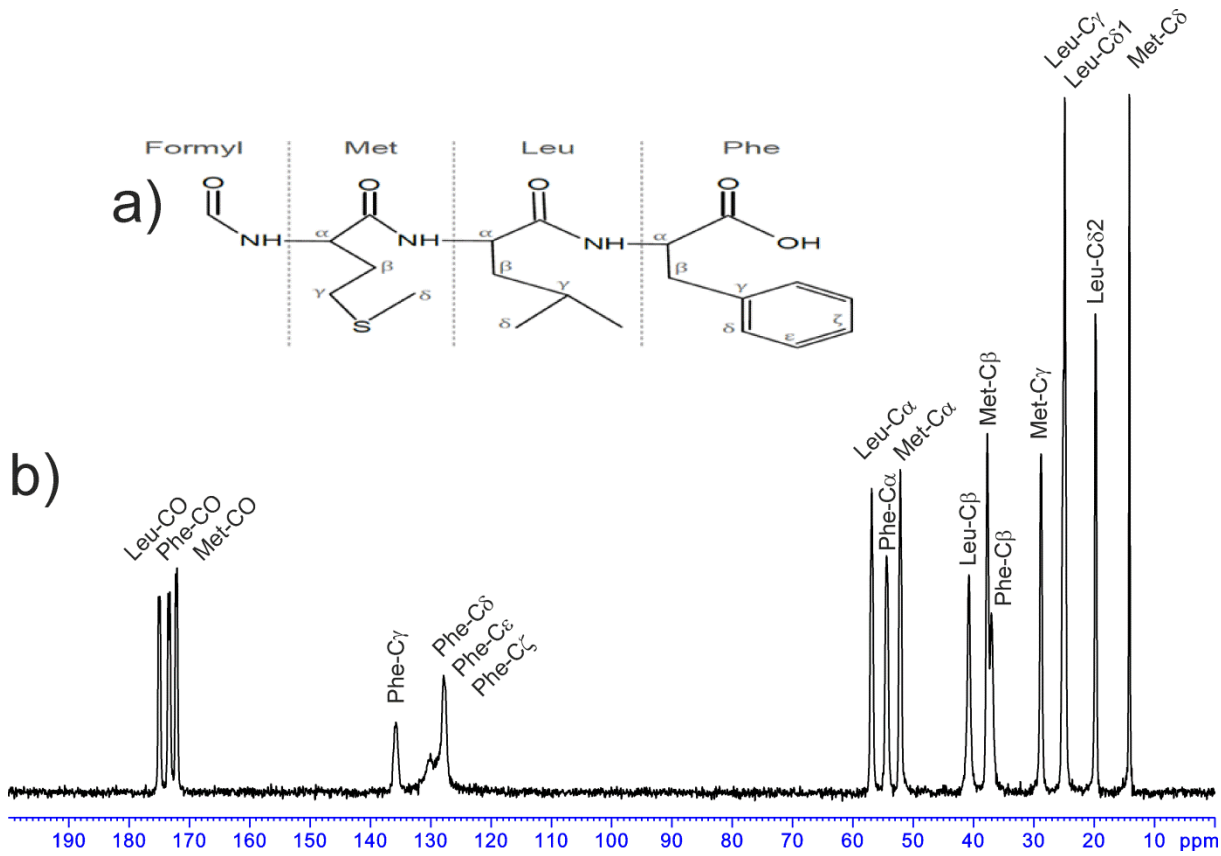

Fig.5. $^{13}C,^{15}N$-f-MLF: molecular structure, and ^{13}C CP-MAS spectra observed at 18.8 T with ν_R = 62.5 kHz. The labelling and assignment of ^{13}C and ^{15}N resonances have been given in ref [27,28]. The 14 resolved resonances used with Hadamard were: L', F', M', F^{γ}, F^{δ} + F^{ε} + F^{ζ}, L^{α}, F^{α}, M^{α}, L^{β}, M^{β} + F^{β}, M^{γ}, L^{γ} + $L^{\delta 1}$, $L^{\delta 2}$, M^{δ}.

We show the ^{13}C-^{13}C 2D spectra of f-MLF corresponding either to the aliphatic part or the full frequency range in Figs **6** or **S12**, respectively. The conventional spectra are shown in Fig.**6a** and **S12a**, whereas the Hadamard ones are in Fig.**6b-d** and **S12b-d**. The long mixing time used with RFDR (Figs.**6a**,**b** and **S12a**,**b**), τ_{mix} = 10.24 ms, leads to the appearance of nearly all cross-peaks, as previously shown in Fig.**4a**,**d**. The conventional acquisition used 256 t_1-steps, and the experimental time was T_{exp} = 280 min with NS = 16. It must be noted that the resolution along F1 is then ca. three times larger than that observed with a 1D CPMAS spectrum. This means that the FIDs were largely truncated along t_1, and that the optimum acquisition time should have been ca. 800 min with three times more t_1 points. With the H_{16} matrix, the experimental time was of only T_{exp} = 34 min, and the sensitivity was multiplied by 4 as we used NS = 64 (Fig.**6b-d**). With the same sensitivity as the conventional experiment, the 2D acquisition time could have been decreased to T_{exp} = 8 min 30 s. In spite of the much shorter acquisition time, the experimental 2D spectra are fundamentally identical. So, the comparison of the two RFDR spectra implies that for the same resolution, the conventional acquisition requires 3*280/8.5 ≈ 100 times more experimental time than the H_{16}-RFDR acquisition. This large decrease of T_{exp} allows recording the build-up curves, which may be impossible with the conventional method. The H_{16}-CP^3 acquisition used a short mixing time of τ_{mix} = 100 µs to limit the ^1H-^1H spin diffusion process (Figs.**6c** and **S12c**). However, in spite of a 100-time shorter mixing time, the RFDR and CP^3 cross-peak patterns are not very different (compare Figs.**6b** and **c** and **S12b** and **c**). It should be also noted that in the CP^3 spectrum, cross-peaks from protonated carbons are much larger than those from quaternary ones. Finally, in Fig.**6d** and **S12d** we show that a similar 2D spectra can be obtained with the

H_{16}-DQF-$BR2_2^1$ recoupling, with same acquisition time. Actually, the H_{16}-CP^3 and H_{16}-DQF-$BR2_2^1$ spectra (Figs.**6c** and **d**) only display correlations between directly bonded carbons because they use small τ_{mix} = 100 and 512 µs, respectively, contrary to H_{16}-RFDR with large τ_{mix} = 10.24 ms (Fig.**6b**) with all remote connections.

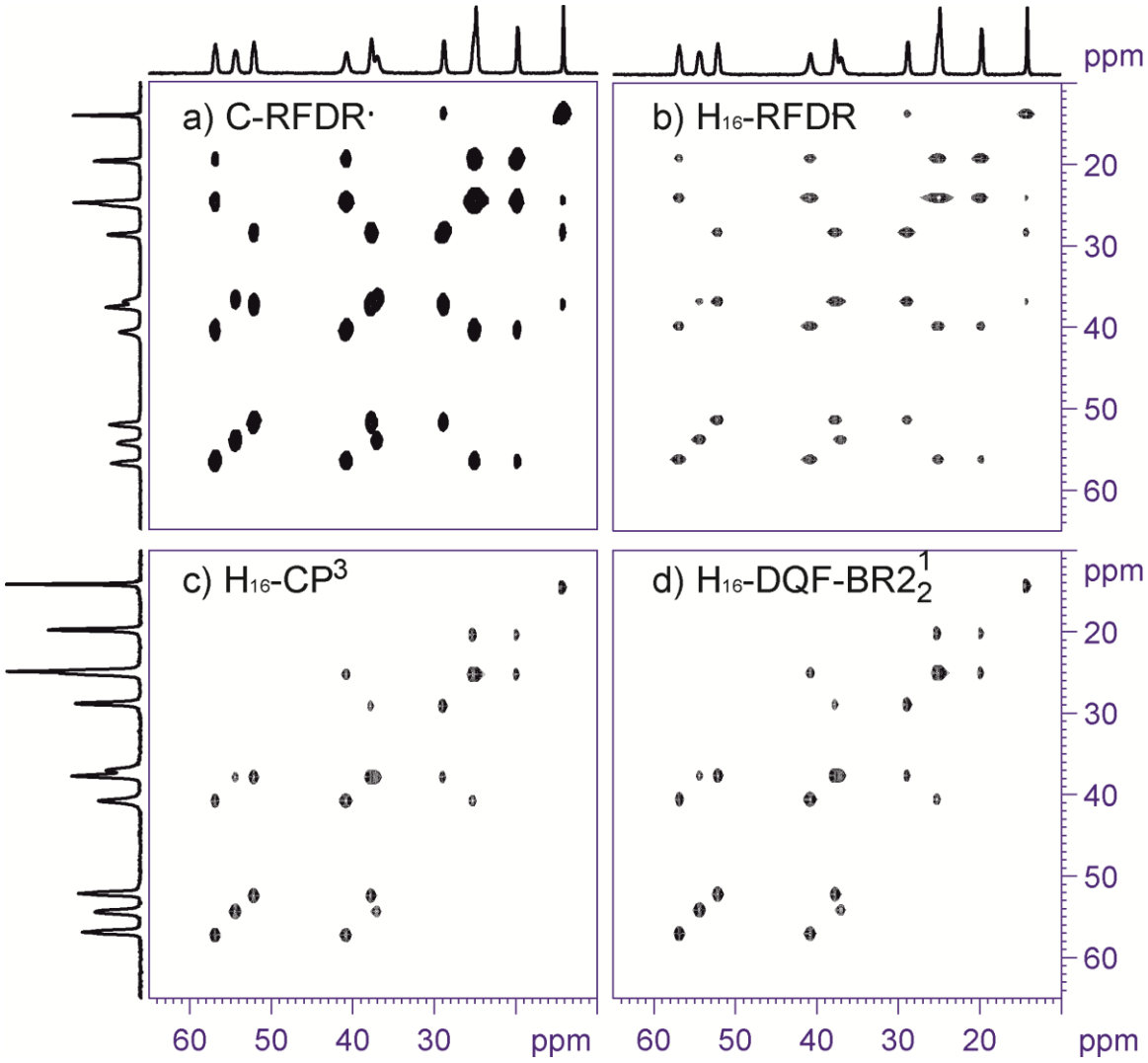

Fig.6. Aliphatic part of ^{13}C-^{13}C 2D spectra of f-MLF recorded at 18.8 T with ν_R = 62.5 kHz, RD = 2 s. (a) Conventional-RFDR acquired with 256 t_1-steps in indirect dimension, ν_{RFDR} = 178 kHz, τ_{mix} = 10.24 ms = 640T_R, NS = 16, T_{exp} = 280 min. (b-d) BW_{FWHM} = 150 Hz, τ_{sp} = 6 ms, NS = 64, T_{exp} = 34 min. (b) H_{16}-RFDR, τ_{mix} = 10.24 ms; (c) H_{16}-CP^3, τ_{mix} = 100 µs, τ_{CP1} = 1500, τ_{CP2} = τ_{CP3} = 200 µs; (d) H_{16}-DQF-$BR2_2^1$, τ_{mix} = 512 µs.

V. Conclusions

In this article we have shown that a multi-selective excitation with Hadamard encoding is a powerful tool for 2D acquisition of ^{13}C-^{13}C homo-nuclear correlations. This method is not designed to improve the sensitivity, but rather to reduce the experiment time, provided there is ***sufficient sensitivity***. Therefore, it allows fast acquisition of such 2D spectra in labeled molecules.

Nevertheless, there are several requirements that must be satisfied.

First, the 1D ^{13}C spectra must be recorded in advance in order to obtain the prior knowledge of the resonance frequencies.

Secondly, this method mainly applies to molecules of small or moderate size which produce a limited number of resonances. Indeed, the main limitation of the Hadamard methods in solids resides in the length of the encoding pulses, which results from a compromise between the selectivity and the sensitivity due to relaxation losses. For this reason, these methods should mainly be used with sparse spectra, profiting from the increased separation of the resonances at high magnetic fields. In the case of ^{13}C-^{13}C HOMCOR experiments, we give a simple rule that allows directly setting the optimum length of the selective pulses, versus the minimum separation of the resonances in the indirect dimension. It cannot be applied to proteins, contrary to the covariance method, which is another way to decrease the acquisition time of HOMCOR spectra in liquid [29–33] or solid samples.[34–37]

Thirdly, this method better applies to the case of narrow resonances, that are fully resolved. It should not be used with broad resonances resulting from distribution of surroundings or quadrupolar nuclei.

Fourth, its advantage is maximum in the case of narrow resonances that are spread over a large frequency range, because this requires numerous t_1 steps with the conventional method, whereas the size of the Hadamard matrix is only related to the number of resonances. One main application of this method is that of ^{13}C-^{13}C spectra of well crystallized samples, especially when they are recorded at very high magnetic fields.

Fifth, it must be mentioned that Hadamard experiments require very linear rf-amplifiers in the low rf-regime to allow the simultaneous optimization of the selective π-pulses for all resonances and all elements of the H_n Hadamard encoding matrix.

The demonstration has been performed on a U-^{13}C-^{15}N histidine hydrochloride monohydrate. sample, and it allowed recording each point of the build-up curves of the ^{13}C-^{13}C cross-peaks within 4 min 35 s, which is very difficult with conventional methods. We have also shown on U-^{13}C-^{15}N f-MLF sample that the method can be applied to molecules with 14 ^{13}C resonances with a minimum frequency separation of 240 Hz at 18.8T. It must be noted that for some pairs of carbon atoms (e.g. M^{β} & F^{β} or L^{γ} & $L^{\delta 1}$) this difference is much smaller, but in this case each of these pairs has been consider as a single species for the selective excitation. However, it has also to be noted that in these cases the conventional acquisition could not either separate the individual species (Fig.**6a**).

Supplementary Information. Figures S1-S11, Table S1, and pulse programs for the three HOMCOR sequences.

VI. Acknowledgments

PP is grateful for funding from the MOBILITY PLUS program (grant no. 1630/MOB/V/2017/0). Institut Chevreul (FR 2638), Ministère de l'Enseignement Supérieur et de la Recherche, Région Hauts-de-France and the European Union (FEDER/ERDF) are acknowledged for supporting and partially funding this work. Financial and technical supports from the TGIR-RMN-THC FR 3050 CNRS for conducting the research are gratefully acknowledged. Authors also acknowledge contract CEFIPRA nos. 85208-E, PRC CNRS-NSFC, ANR-14-CE07-0009-01 and ANR-17-ERC2-0022 (EOS). OL acknowledges financial support from Institut Universitaire de France (IUF).

VII. References

[1] S. Sibisi, J. Skilling, R.G. Brereton, E.D. Laue, J. Staunton, Maximum entropy signal processing in practical NMR spectroscopy, *Nature*. 311 (**1984**) 446–447. doi:10.1038/311446a0.

[2] K. Kazimierczuk, V. Orekhov, Non-uniform sampling: post-Fourier era of NMR data collection and processing: Non-uniform sampling, *Magn. Reson. Chem*. 53 (**2015**) 921–926. doi:10.1002/mrc.4284.
[3] J.C.J. Barna, E.D. Laue, Conventional and exponential sampling for 2D NMR experiments with application to a 2D NMR spectrum of a protein, *J. Magn. Reson*. 75 (**1987**) 384-389. doi:10.1016/0022-2364(87)90047-3.
[4] Ē. Kupče, R. Freeman, Fast multi-dimensional Hadamard spectroscopy, *J. Magn. Reson*. 163 (**2003**) 56–63. doi:10.1016/S1090-7807(03)00036-3.
[5] Ē. Kupče, R. Freeman, Multisite correlation spectroscopy with soft pulses. A new phase-encoding scheme, *J. Magn. Reson.* A 105 (**1993**) 310–315.
[6] E. Kupče, T. Nishida, R. Freeman, Hadamard NMR spectroscopy, *Prog. Nucl. Magn. Reson. Spectrosc*. 42 (**2003**) 95–122. doi:10.1016/S0079-6565(03)00022-0.
[7] Ē. Kupče, R. Freeman, Two-dimensional Hadamard spectroscopy, *J. Magn. Reson.* 162 (**2003**) 300–310. doi:10.1016/S1090-7807(02)00196-9.
[8] J. Ashida, Ē. Kupče, J.-P. Amoureux, Hadamard NMR spectroscopy in solids, *J. Magn. Reson*. 178 (**2006**) 129–135. doi:10.1016/j.jmr.2005.09.001.
[9] Ē. Kupče, J. Trébosc, B. Perrone, O. Lafon, J.-P. Amoureux, Recording 13C-15N HMQC 2D sparse spectra in solids in 30 s, *J. Magn. Reson*. 288 (**2018**) 76–83. doi:10.1016/j.jmr.2018.01.018.
[10] V.M.R. Kakita, E. Kupče, J. Bharatam, Solid-state Hadamard NMR spectroscopy: Simultaneous measurements of multiple selective homonuclear scalar couplings, *J. Magn. Reson*. 251 (**2015**) 8–12. doi:10.1016/j.jmr.2014.11.006.
[11] M. Shen, B. Hu, O. Lafon, J. Trébosc, Q. Chen, J.-P. Amoureux, Broadband finite-pulse radio-frequency-driven recoupling (fp-RFDR) with (XY8)41 super-cycling for homo-nuclear correlations in very high magnetic fields at fast and ultra-fast MAS frequencies, *J. Magn. Reson*. 223 (**2012**) 107–119. doi:10.1016/j.jmr.2012.07.013.
[12] R. Zhang, Y. Nishiyama, P. Sun, A. Ramamoorthy, Phase cycling schemes for finite-pulse-RFDR MAS solid state NMR experiments, *J. Magn. Reson*. 252 (**2015**) 55–66. doi:10.1016/j.jmr.2014.12.010.
[13] P. Paluch, T. Pawlak, A. Jeziorna, J. Trébosc, G. Hou, A.J. Vega, J.-P. Amoureux, M. Dracinsky, T. Polenova, M.J. Potrzebowski, Analysis of local molecular motions of aromatic sidechains in proteins by 2D and 3D fast MAS NMR spectroscopy and quantum mechanical calculations, *Phys. Chem. Chem. Phys.* 17 (**2015**) 28789–28801. doi:10.1039/C5CP04475H.
[14] F.M. Mulder, W. Heinen, M. van Duin, J. Lugtenburg, H.J.M. de Groot, Spin diffusion with ^{13} C selection and detection for the characterization of morphology in labeled polymer blends with MAS NMR, *J. Am. Chem. Soc*. 120 (**1998**) 12891–12894. doi:10.1021/ja9809511.
[15] A. Lange, S. Luca, M. Baldus, Structural Constraints from Proton-Mediated Rare-Spin Correlation Spectroscopy in Rotating Solids, *J. Am. Chem. Soc*. 124 (**2002**) 9704–9705. doi:10.1021/ja026691b.
[16] I. de Boer, L. Bosman, J. Raap, H. Oschkinat, H.J.M. de Groot, 2D 13C-13C MAS NMR correlation spectroscopy with mixing by true 1H spin diffusion reveals long-range intermolecular distance restraints in ultra-high magnetic field, *J. Magn. Reson*. 157 (**2002**) 286–291. doi:10.1006/jmre. 2002.2588.
[17] M. Aluas, C. Tripon, J.M. Griffin, X. Filip, V. Ladizhansky, R.G. Griffin, S.P. Brown, C. Filip, CHHC and 1H–1H magnetization exchange: Analysis by experimental solid-state NMR and 11-spin density-matrix simulations, *J. Magn. Reson.* 199 (**2009**) 173–187. doi:10.1016/j.jmr.2009.04.013.
[18] T. Kobayashi, I.I. Slowing, M. Pruski, Measuring long-range ^{13}C-^{13}C correlations on a surface under natural abundance using Dynamic Nuclear Polarization-Enhanced Solid-State Nuclear Magnetic Resonance, *J. Phys. Chem*. C. 121 (**2017**) 24687–24691. doi:10.1021/acs.jpcc.7b08841.
[19] M. Wilhelm, H. Feng, U. Tracht, H.W. Spiess, 2D CP/MAS 13C isotropic chemical shift correlation established by 1H spin diffusion, *J. Magn. Reson*. 134 (**1998**) 255–260. doi:10.1006/jmre.1998. 1512.

[20] B. Hu, L. Delevoye, O. Lafon, J. Trébosc, J.-P. Amoureux, Double-quantum NMR spectroscopy of 31P species submitted to very large CSAs, *J. Magn. Reson*. 200 (**2009**) 178–188. doi:10.1016/j.jmr.2009.06.020.

[21] M. Edén, D. Zhou, J. Yu, Improved double-quantum NMR correlation spectroscopy of dipolar-coupled quadrupolar spins, *Chem. Phys. Lett*. 431 (**2006**) 397–403. doi:10.1016/j.cplett.2006.09.081.

[22] I. Schnell, Dipolar recoupling in fast-MAS solid-state NMR spectroscopy, *Prog. Nucl. Magn. Reson. Spectrosc*. 45 (**2004**) 145–207. doi:10.1016/j.pnmrs.2004.06.003.

[23] G. Teymoori, B. Pahari, B. Stevensson, M. Edén, Low-power broadband homonuclear dipolar recoupling without decoupling: Double-quantum 13C NMR correlations at very fast magic-angle spinning, *Chem. Phys. Lett*. 547 (**2012**) 103–109. doi:10.1016/j.cplett.2012.07.053.

[24] G. Teymoori, B. Pahari, M. Edén, Low-power broadband homonuclear dipolar recoupling in MAS NMR by two-fold symmetry pulse schemes for magnetization transfers and double-quantum excitation, *J. Magn. Reson*. 261 (**2015**) 205–220. doi:10.1016/j.jmr.2015.09.004.

[25] Q. Wang, B. Hu, O. Lafon, J. Trébosc, F. Deng, J.-P. Amoureux, Double-quantum homonuclear NMR correlation spectroscopy of quadrupolar nuclei subjected to magic-angle spinning and high magnetic field, *J. Magn. Reson*. 200 (**2009**) 251–260. doi:10.1016/j.jmr.2009.07.009.

[26] Z. Yu, A. Zheng, Q. Wang, L. Chen, J. Xu, J.-P. Amoureux, F. Deng, Insights into the dealumination of zeolite HY revealed by sensitivity-enhanced 27Al DQ-MAS NMR spectroscopy at high field, *Angew. Chem. Int. Ed*. 49 (**2010**) 8657–8661. doi:10.1002/anie.201004007.

[27] K. Mao, M. Pruski, Directly and indirectly detected through-bond heteronuclear correlation solid-state NMR spectroscopy under fast MAS, *J. Magn. Reson*. 201 (**2009**) 165–174. doi:10.1016/j.jmr.2009.09.004.

[28] S.M. Althaus, K. Mao, J.A. Stringer, T. Kobayashi, M. Pruski, Indirectly detected heteronuclear correlation solid-state NMR spectroscopy of naturally abundant 15N nuclei, *Solid State Nucl. Magn. Reson*. 57–58 (**2014**) 17–21. doi:10.1016/j.ssnmr.2013.11.001.

[29] F. Zhang, R. Brüschweiler, Spectral Deconvolution of Chemical Mixtures by Covariance NMR, *ChemPhysChem*. 5 (**2004**) 794–796. doi:10.1002/cphc.200301073.

[30] F. Zhang, R. Brüschweiler, Indirect Covariance NMR Spectroscopy, *J. Am. Chem. Soc*. 126 (**2004**) 13180–13181. doi:10.1021/ja047241h.

[31] N. Trbovic, S. Smirnov, F. Zhang, R. Brüschweiler, Covariance NMR spectroscopy by singular value decomposition, *J. Magn. Reson.* 171 (**2004**) 277–283. doi:10.1016/j.jmr.2004.08.007.

[32] R. Brüschweiler, F. Zhang, Covariance nuclear magnetic resonance spectroscopy, *J. Chem. Phys*. 120 (**2004**) 5253–5260. doi:10.1063/1.1647054.

[33] R. Brüschweiler, Theory of covariance nuclear magnetic resonance spectroscopy, *J. Chem. Phys*. 121 (**2004**) 409. doi:10.1063/1.1755652.

[34] B. Hu, J.-P. Amoureux, J. Trébosc, M. Deschamps, G. Tricot, Solid-state NMR covariance of homonuclear correlation spectra, *J. Chem. Phys*. 128 (**2008**) 134502. doi:10.1063/1.2884341.

[35] O. Lafon, B. Hu, J.-P. Amoureux, P. Lesot, Fast and high-resolution stereochemical analysis by non-uniform sampling and covariance processing of anisotropic natural abundance 2D 2H NMR datasets, *Chem. Eur. J.* 17 (**2011**) 6716–6724. doi:10.1002/chem.201100461.

[36] Y. Li, B. Hu, Q. Chen, Q. Wang, Z. Zhang, J. Yang, I. Noda, J. Trébosc, O. Lafon, J.-P. Amoureux, F. Deng, Comparison of various sampling schemes and accumulation profiles in covariance spectroscopy with exponentially decaying 2D signals, *The Analyst*. 138 (**2013**) 2411. doi:10.1039/c3an36375a.

[37] Y. Qian, M. Shen, J.-P. Amoureux, I. Noda, B. Hu, The dependence of signal-to-noise ratio on number of scans in covariance spectroscopy, *Solid State Nucl. Magn. Reson*. 59–60 (**2014**) 31–33. doi:10.1016/j.ssnmr.2014.02.002.